Materials Examination of the Vertical Stabilizer from American Airlines Flight 587

Matthew R. Fox[1], Carl R. Schultheisz[1], James R. Reeder[2], and Brian J. Jensen[2]

[1]National Transportation Safety Board, 490 L'Enfant Plaza, SW, Washington, DC 20594
[2]NASA Langley Research Center, Hampton, VA 23681

Keywords: Failure analysis, CFRP, composites, American Airlines Flight 587

Abstract

The first in-flight failure of a primary structural component made from composite material on a commercial airplane led to the crash of American Airlines Flight 587. As part of the National Transportation Safety Board investigation of the accident, the composite materials of the vertical stabilizer were tested, microstructure was analyzed, and fractured composite lugs that attached the vertical stabilizer to the aircraft tail were examined. In this paper the materials testing and analysis is presented, composite fractures are described, and the resulting clues to the failure events are discussed.

Introduction

On November 12, 2001, shortly after taking off from Kennedy International Airport, the composite vertical stabilizer and rudder separated from the fuselage of American Airlines Flight 587, rendering the airplane uncontrollable. The Airbus A300-600 airplane crashed into a neighborhood in Belle Harbor, New York, killing all 260 persons aboard the airplane and 5 persons on the ground. This accident was unique partly in that it was the first time a primary structural component fabricated out of composite material failed in flight on a commercial airplane.

As a result of the analysis of the facts learned during the course of the nearly 3-year long investigation of the accident, the National Transportation Safety Board determined that the probable cause of the accident was, "the in-flight separation of the vertical stabilizer as a result of the loads beyond ultimate design that were created by the first officer's unnecessary and excessive rudder pedal inputs. Contributing to these rudder pedal inputs were characteristics of the Airbus A300-600 rudder system design and elements of the American Airlines Advanced Aircraft Maneuvering Program [1]."

Analysis of the flight data recorder revealed the airplane had performed a series of yawing maneuvers in the seconds before separation of the vertical stabilizer, and the separation of the vertical stabilizer occurred while the airplane was pointed to the left of its flight path. This orientation would have produced a bending moment on the vertical stabilizer leading to tension on the right-side attachments and compression on the left.

The separated pieces of the vertical stabilizer and rudder were recovered away from the main crash site mainly from the water of Jamaica Bay. The vertical stabilizer was largely intact, and had separated from the fuselage by fractures at the lower end where it had been connected to the fuselage. Many fractured pieces of the rudder were recovered near, but mostly fractured from, the vertical stabilizer. Although a detailed examination of the rudder was completed during the accident investigation, performance analysis of the flight recorder data indicated that the rudder performed as designed through the accident sequence until the vertical stabilizer separated from the fuselage, and loads

analysis indicated that the vertical stabilizer would fail before the rudder. Thus, the rudder failure was secondary to the failure of the vertical stabilizer. As part of the overall investigation into the accident, the composite materials of the vertical stabilizer were examined and tested, and a detailed examination of the fractures in the vertical stabilizer was conducted in order to determine the failure mechanism and direction of fracture propagation where possible, including assessing the possibility of any pre-existing damage or fatigue cracking.

Using accident loads derived from analysis of recorded flight data, three subcomponent tests were conducted on vertical stabilizer aft lugs from an unused skin panel and from another airplane. Fracture patterns for these three test specimens were compared to the corresponding structure on the accident airplane.

In this paper, the structure of the vertical stabilizer is described. Next, results of the materials testing and microstructural examination are shown. Then, fractography of the vertical stabilizer is presented, and the interpretation of the results toward understanding the failure is discussed. Finally, fractographic examination results of the three subcomponent tests are presented and significance of the fracture features are discussed.

Description of the Structure

Development of the Airbus A300-600 model began in 1980, and certification occurred in 1984. The vertical stabilizer and rudder for this model airplane had a symmetric airfoil shape. The vertical stabilizer and rudder were 27 feet 3 inches tall. From leading edge to trailing edge the width of the vertical stabilizer and rudder was 25 feet at the base and 10 feet 2 inches at the tip. The accident airplane was delivered new in 1988

Vertical Stabilizer Structure

The vertical stabilizer design for the Airbus A300-600 series airplane is a stiffened box with removable leading edge fairings and trailing edge panels. An internal view drawing of the vertical stabilizer is shown in Figure 1. The stiffened box consists of two integrally stiffened skin panels for the left and right sides, spars for the forward and aft sides, and closure ribs at the upper and lower ends. The integral stiffeners in the skin panels consist of 24 "I"-shaped stringers that extend spanwise parallel to the aft spar, numbered from the aft to forward. Internal stiffeners for the box consist of a center spar at the lower end of the span and 16 ribs, not including the two closure ribs. The ribs are numbered from the lower end upward starting with the lower closure rib. The components of the box are riveted together, and the leading edge fairings and trailing edge panels are attached with threaded fasteners.

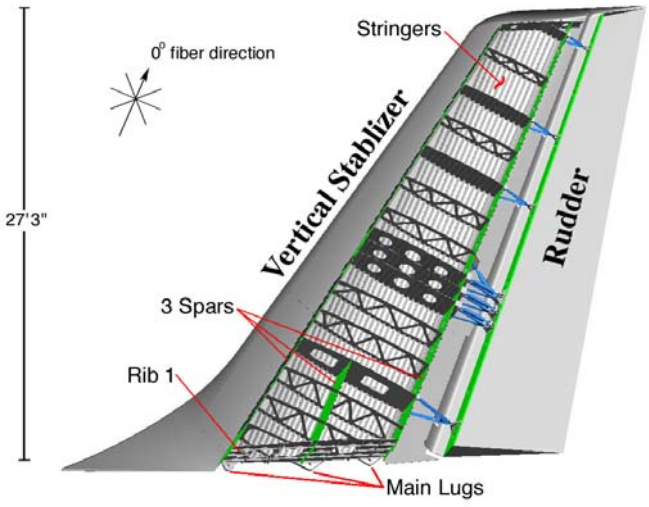

Figure 1: Airbus A300-600 vertical stabilizer construction.

Except for the fasteners, lightning protection strips, and trailing edge panel support frames, the vertical stabilizer is designed to be made entirely of composite materials. The stiffened box of the vertical stabilizer is a solid carbon-fiber reinforced polymer (CFRP) laminate composed of T300 carbon fibers in a CIBA 913 epoxy matrix. The laminate includes both unidirectional tape and eight-harness satin fabric layers in the construction. The zero-

degree fibers of the fabric and tape layers in the composite are oriented parallel to the stringers and the aft spar, which are at an angle of 33.3 degrees aft of vertical. The leading edge fairings and the trailing edge panels for the vertical stabilizer are sandwich composites having a Nomex honeycomb core with glass-fiber reinforced polymer (GFRP) facesheets for the leading edge fairings and both GFRP and CFRP facesheets for the trailing edge panels.

The main connections for attaching the vertical stabilizer to the fuselage are designed as six CFRP lugs (main lugs) on the lower end of the vertical stabilizer that connect by bolts approximately 2 inches in diameter to six metal clevis fittings on the fuselage. A schematic view of the typical assembly cross-section is shown in Figure 2 (drawing of lug cross-section). After the assembly is cured during manufacturing, the lug attachment bolt holes are core-drilled out. Three main lugs extend from the lower end of each of the two vertical stabilizer skin panels. At the thickest point, the main lugs are approximately 1.62 inches, 2.48 inches, and 2.17 inches thick for the forward, center, and aft lugs, respectively. The aft lugs alone each have more than 170 layers composed of approximately 50 percent ±45-degree fabric, 25 percent 0/90-degree fabric, and 25 percent 0-degree tape. The thickness of each lug decreases as plies are dropped in the lug-to-skin transition area. The skin layers are made of ±45-degree fabric. The I-shaped stringers have 0-degree tape at the caps and ±45-degree fabric in the web.

Each lug contains two separate pieces that are cured separately before the final assembly. In the final assembly, the outer precured half is laid down, followed in order by the skin layers, the inner precured half, the compensation layers, the rib 1 attach flange, the stringer outer flange (tape) layers, and the stringer module layers.

Six smaller composite lugs (transverse lugs) attach the vertical stabilizer to the fuselage by lateral yokes. Two of these transverse lugs extend from the lower end of each of the three spar webs. These lugs are approximately 0.47 inch thick.

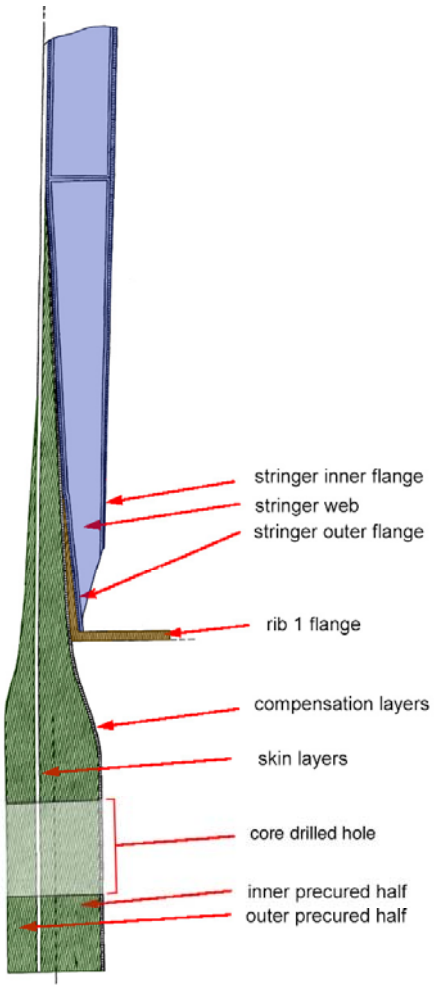

Figure 2: Drawing of main lug cross-section.

Materials Testing and Microstructural Examination

The materials testing and microstructural examination of samples of the accident vertical stabilizer were completed primarily at the National Aeronautics and Space Administration's Langley Research Center (NASA Langley) in Hampton, Virginia. Some testing and microscopy were completed at the Airbus Industrie's composites technology division in Bremen, Germany. Details of the materials characterization and testing are provided in reference 2.

Samples were selected from multiple locations on the vertical stabilizer for materials testing and microscopic examination to determine chemical composition, extent of cure, glass transition temperature (T_g), fiber and void volume fractions, and ply stacking sequence (layup). On the right side

skin panel, four samples were cut from undamaged areas near the aft spar plus two samples were cut from damaged areas in the forward and aft lower attachment lugs. On the left side skin panel, three samples were cut from undamaged areas near the forward spar and one sample was cut from a damaged area near the left forward lug. One sample each from the forward, center, and aft spar, and from ribs 1 and 3 were cut from undamaged areas. Testing of samples from each area included differential scanning calorimetry (DSC) and infrared spectroscopy (IR). Samples from one area were tested using dynamic mechanical analysis (DMA) and modulated differential scanning calorimetry (MDSC). The fiber volume fraction, void volume fraction, and layup in each area were determined using microscopic examination of polished cross-sections.

The curing temperature for the CFRP was specified to be 250 degrees Fahrenheit. According to Airbus material qualification data, the onset glass transition temperature ($T_{g\text{-}onset}$) was 144 degrees Celsius in the dry condition and was 122 degrees Celsius after exposure to a climate of 50 percent relative humidity (corresponding to a moisture content of 0.7 weight percent). According to the engineering drawings, the fiber volume fraction for the CFRP was 60% ± 4%. The maximum volume fraction porosity permitted in the cross-section was 2.5 percent.

The chemical composition of samples from each area was assessed using IR spectroscopy, measuring total attenuated reflectance through a microscope. The results were typical for this composite material with no significant variances in the spectra for each specimen.

The extent of cure and the T_g of the sample from the upper end of the right skin panel (sample RS4) were analyzed using MDSC, DMA, and DSC. Portions of sample RS4 were tested in the as-received condition and after drying. The moisture content for the as-received condition was approximately 0.58 percent. The MDSC results showed an average residual heat value of 4.5 joules per gram, which corresponded to an extent of cure greater than 97 percent. The DMA results show that in the as-received condition, the $T_{g\text{-}onset}$ measured 134 degrees Celsius, which was between the qualification values of 144 degrees Celsius for the dry condition and 122 degrees Celsius for the 50 percent relative humidity (0.7 percent moisture content) condition. The portion of sample RS4 that was tested in the dry condition had a $T_{g\text{-}onset}$ of 149 degrees Celsius.

The extent of cure and the T_g of each sample, including sample RS4, was assessed using DSC. No significant variance was observed in the results among all the samples. Results indicated that the extent of cure for each sample was sufficient.

Sections of each sample were cut, mounted, and polished for microstructural examination and quantitative analysis. The cross-sections from the vertical stabilizer were prepared and analyzed at NASA Langley and at Airbus Industrie. A typical cross-sectional view is shown in Figure 3 for a sample from the lower end of the right skin panel (sample RS1). The cross-section shown is in a plane oriented parallel to the plus or minus 45-degree fiber direction. Fiber and void

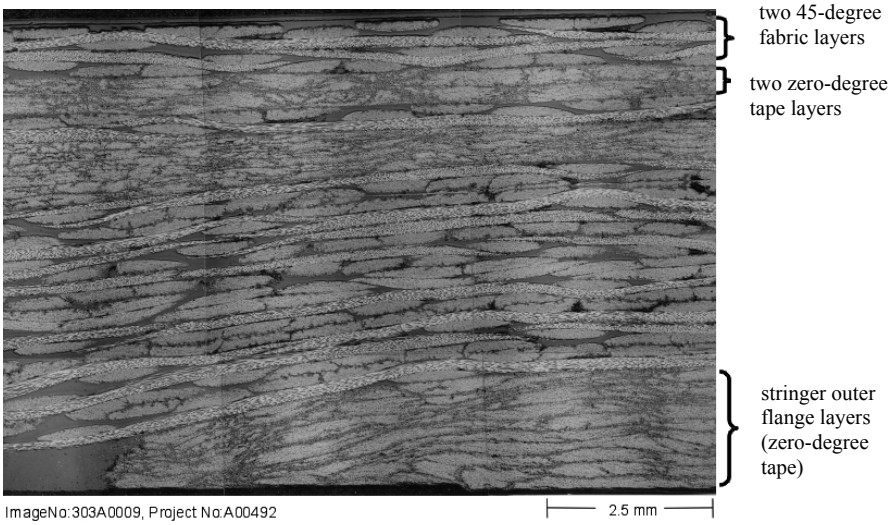

Figure 3: Microstructure of sample RS1.

content were determined using computer optical image analysis of polished micrographs. The layup in each sample was determined from optical micrographs of the specimens that were assembled into mosaics such as that of Figure 3.

Results of the microstructural examination and analysis indicated that the composite structure of the vertical stabilizer was constructed to the desired fiber volume fraction with acceptable void content. No evidence of microcracking was observed. The observed layups were compared to the engineering drawings obtained from the manufacturer, and among the 15 samples, only one sample from the right forward lug (sample RF4) showed any discrepancies. Within the 124 layers of sample RF4, 2 layers had orientations that were different from the drawing. Also, two layers appeared to be missing from one position through the thickness, but two additional layers were present at another position. The total number of layers for each orientation in sample RF4 was correct, and the discrepancies represented a small fraction of the total number of layers.

Fractographic Examination Procedures and Challenges

For most common airplane structural metals, visual inspection or low-power magnification is often sufficient to determine fracture mechanism and direction. For metals, the fracture plane, surface roughness, radial marks, chevrons, shear lips, and general deformation when present all provide macroscopic clues to the fracture mechanisms, direction of fracture propagation, and relative motion of mating surfaces. Preexisting cracks in metals often show staining or changes in color associated with corrosion [3]. Using these clues, large areas of damaged structure can be examined relatively quickly by an experienced investigator to identify fracture origins and areas requiring closer inspection.

The fractographic examination of the composite fractures in the accident vertical stabilizer presented a challenge in that it was more extensive than would typically be required for an overstress fracture of a similar metal structure. Visual clues to preexisting fractures, such as flat fracture features with curving boundaries or staining from corrosion that can be readily observed in structural metals, generally are not readily visible in composites. Furthermore, the visual cues to fracture propagation directions that are sometimes apparent in composite structures, such as crack branching in translaminar fractures (fractures that break fibers) or banding in delaminations (fractures between layers), were not apparent in many of the fractures of interest. In determining the failure mechanism and directions in the vertical stabilizer and rudder during the accident investigation, fine fracture features were examined at high magnification across relatively large areas of the fracture surfaces in order to determine fracture mechanisms and propagation directions, a time-consuming process for the failure investigation. However, since fatigue fractures and other preexisting cracks may appear similar during a macroscopic examination, the detailed inspection using high magnification was required to complete the fractographic analysis.

The fractographic examination of the translaminar fractures and delaminations of the vertical stabilizer and rudder incorporated visual examination and scanning electron microscopy (SEM). The visual examination included the documentation of the macroscopic fracture features. The documentation included mapping of fractures, which could be used to aid in identifying fracture propagation directions from crack branching patterns. Also, macroscopic indications of translaminar fracture under tension or compression were documented. On delaminations, surfaces were examined for changes in reflectivity, which could indicate changes in fracture mechanism or mode [4]. However, for most of the fracture surfaces, SEM was required to determine the fracture mechanism and fracture propagation direction.

SEM examination of translaminar fracture surfaces was used to determine the fracture mechanism and propagation directions, and SEM examination of delamination surfaces was used to identify the layers

involved, fracture mechanisms, modes of fracture, and propagation directions. Additionally, results of the examination were used to check the construction against the manufacturing drawings and to determine how the fractures related to the loading of the overall structure.

Over 300 SEM photographs were taken of translaminar fractures in the main attachment areas of the vertical stabilizer, and more than 150 square inches of delamination surface areas were examined at high magnification. Examined fracture surfaces were coated with a conductive layer of gold and palladium. For translaminar fractures intersecting the lug attachment hole, the entire fracture surfaces were examined at high magnification, and for translaminar fractures above the lug holes, several inches of the fracture were examined at high magnification. Samples for the SEM examination of the delamination surfaces were typically approximately two inches square and were taken from widely spaced areas on the exposed fracture surfaces in an effort to identify the overall trends. Samples were also taken across areas where the delamination surface morphology changed (mostly as a result of the ends of plies in the lay-up) to explore for local differences in stress state or crack propagation direction. Two samples, one from each of the two large delaminations, were not cleaned and were the first ones examined in order to explore the surface for matrix rollers, which would have been an indication of fatigue [5]. Since uncleaned samples were covered in debris, all other fracture surfaces were ultrasonically cleaned in water before coating.

Another challenge for the fractographic analysis was the relatively small amount of fractographic reference material dealing specifically with fabric-reinforced composites. Most of the literature describing fractography of composites focused on unidirectional tape lay-ups. However, fabrics have unique characteristics that lead to features such as more variation in resin content on delamination surfaces and less fiber pullout in translaminar fractures relative to tape-reinforced materials. The presence of woven fabric in the construction led to some interesting phenomena that could be useful in better analyzing composites failures. In the unidirectional lay-ups, river marks were typically only observed in Mode I loading. However, in the fabric construction, river marks also could be found in matrix-rich areas in the vicinity of the bundle crossings, and could be seen in the base of hackles in the transition from a bundle at one orientation to a perpendicular crossing bundle. The river marks in the matrix-rich bundle crossings were used to identify a general direction of fracture propagation upward and aftward for both of the large delaminations (at the forward left and aft left attachments). The use of the river marks at the base of the hackles was explored in the examination of the delaminations at the forward right lug. As composites with fabric reinforcements are being increasingly used in airplane structures, more research is needed in characterizing these fracture surfaces generated under controlled laboratory conditions to assist the failure analyst in interpreting fractographic details.

Fracture Surface Observations and Discussion

The vertical stabilizer was largely intact with no significant areas of skin buckling. An overall view of the vertical stabilizer as it was being recovered from the water of Jamaica Bay is shown in Figure 4. At the lower end, each of the six attachment locations were separated either by fractures that intersected the lug attach hole or by fractures through the

Figure 4: Vertical stabilizer as recovered from Jamaica Bay.

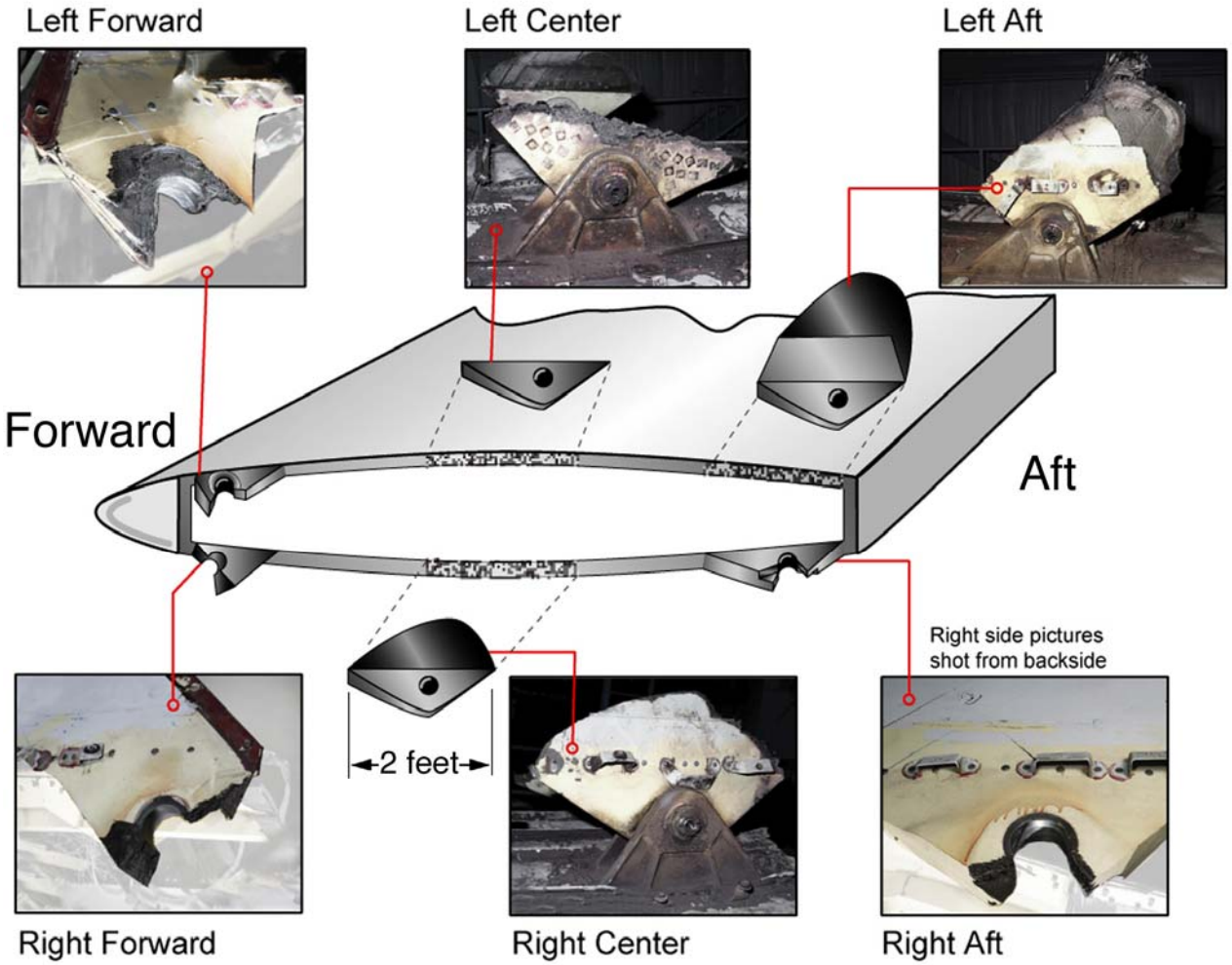

Figure 5: Overall views of main lug fractures with relative locations on vertical stabilizer.

structure above the hole. A schematic drawing of the lower end of the vertical stabilizer is shown in Figure 5, where a general fracture location for each lug is shown with overall views of each of these lug fractures. Portions of rib 1, the rib 1 rib-to-skin attach angle, and the lower end of the forward spar also were fractured. Along the trailing edge, the trailing edge panels were damaged in several locations. A more detailed description of the damage is presented in reference 6.

Description of main lug fractures

The right aft, right forward, and left forward main lugs had translaminar fractures that intersected the attachment hole, and the remaining three main lugs had translaminar fractures in the structure above the lug. Each of the lugs had delaminations in the lug area and/or in the structure above the lug. Details of the fractographic examination are presented in references 7 and 8. Some of the delaminations extended into the main portion of the vertical stabilizer, and the extents of these delaminations were determined using nondestructive inspection (NDI), including ultrasonic inspection and x-ray-computed tomography scanning and imaging. Results of the NDI of the vertical stabilizer are presented in references 9 and 10.

Macroscopic fracture features

The main lug translaminar fractures on the right side of the vertical stabilizer generally had rough fracture features consistent with overstress fracture in primarily tensile loading. Delaminations were observed at the edges of each of the lugs on the right side. The extent of the delaminations as determined using NDI was limited to within the fractured lugs or within approximately four inches of a translaminar fracture.

The right aft lug failed by translaminar fracture through the bolt hole as shown in Figure 6. The translaminar fracture surfaces had a rough appearance consistent with fracture primarily under tensile loading. Fractures on each leg of the lug were on different translaminar planes, and the change in planes occurred near the center of the lug thickness. On the aft side of the bolt hole, the outboard side of the fracture was in a plane nearly perpendicular to the zero-degree fiber direction, and the inboard side of the fracture was in a plane approximately parallel to the 45-degree fiber direction. On the forward side of the bolt hole, the outboard side of the fracture was in a plane approximately parallel to the zero-degree fiber direction, and the inboard side of the fracture was in a plane nearly parallel to rib 1. Bearing damage was observed at the bore surface near both fracture surfaces, as indicated by white unlabeled arrows in Figure 6.

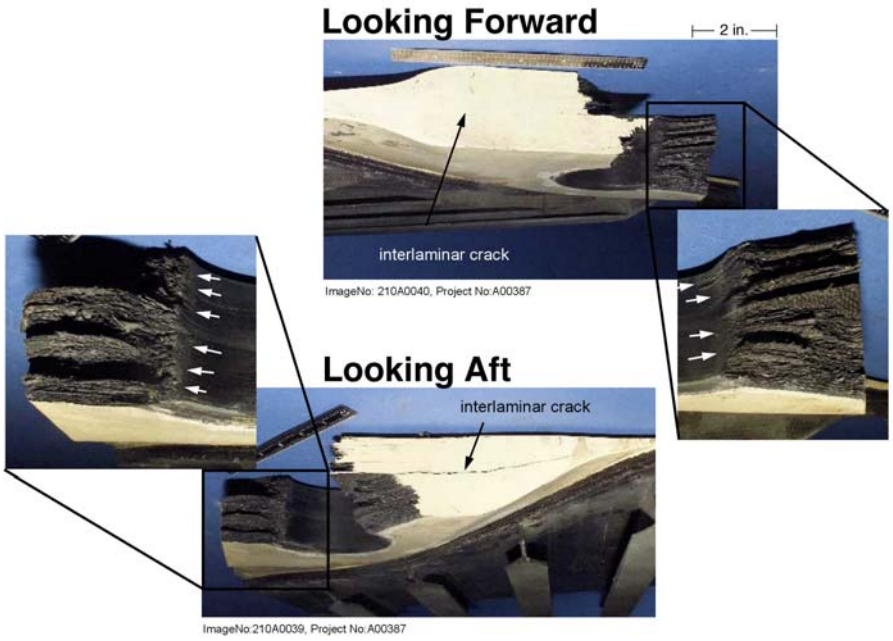

Figure 6: Right aft lug translaminar fractures (pictured from below the lug).

The right center lug failed above the bolt hole in the lug-to skin transition above rib 1. Translaminar fracture features were relatively rough, consistent with overstress fracture under tensile loading.

Fractures on the right forward lug intersected the lug hole. Translaminar fracture features were relatively rough, consistent with overstress fracture under tensile loading. Some evidence of local compressive loading was observed near the aft side of the lug, indicating that fracture first occurred at the forward side of the lug, and then the lower ligament hinged about the aft side of the lug.

The main lug translaminar fractures on the left side of the vertical stabilizer also generally had rough fracture features consistent with overstress fracture in primarily tensile loading, but they also showed indications of bending to the left. The left forward lug had multiple delaminations in the lug area and an impression on the left side corresponding to contact with the fuselage attachment clevis. The impression indicates the left skin panel of the vertical stabilizer bent to the left, damage that can only be explaned if the right side skin panel was already separated from the fuselage. The left forward lug also had a delamination extending upward into the structure up to 43 inches from the lower end. The left center lug had an area with compression fracture features at the outboard side of the translaminar

fracture, consistent with bending loads to the left. The left aft lug had delaminations extending up to 37 inches from the lower end. Multiple delaminations through the thickness were present in the lug-to-skin transition area, allowing most of the precured halves of the lug to separate from the rest of the structure.

Microscopic fracture features

On translaminar fractures, the ends of some fibers were oriented roughly perpendicular to the fracture plane. A typical SEM view of these fiber ends on one of the translaminar fracture surfaces is shown in Figure 7. Fiber ends such as those shown in Figure 7 were examined using SEM to help determine the fracture mechanism and propagation direction. For fibers having radial patterns indicative of tensile fracture, the local fracture propagation direction could be determined from the direction of the radial pattern of several fibers [11, 12]. Then, general directions of fracture propagation for the translaminar fractures could be determined by averaging the directions indicated by the radial patterns across many areas of the fracture surfaces. Also, since fatigue and overstress fractures can appear similar from a macroscopic view, the microscopic examination of the fracture surfaces included looking for evidence of fatigue such as rounded edges on fiber ends [13] or striations in the matrix [5, 12, 14], however, no evidence of fatigue was observed on any of the translaminar fracture surfaces.

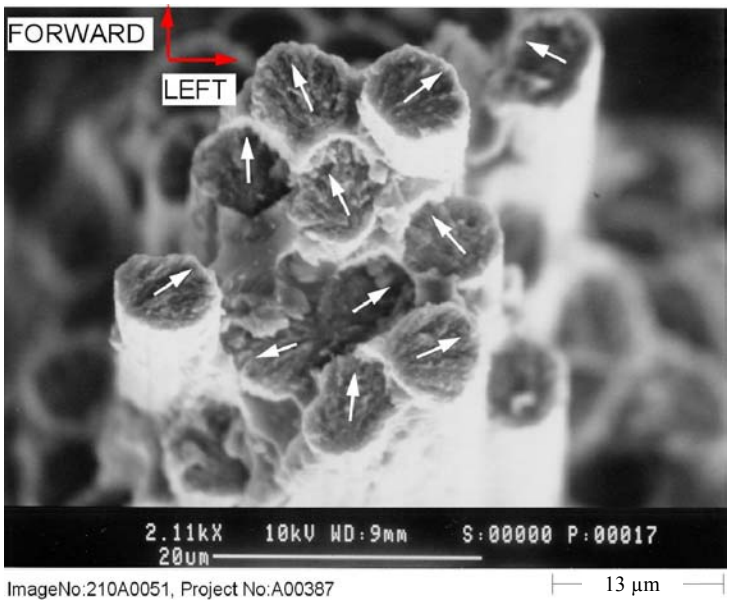

Figure 7: Fractured carbon fibers showing crack growth directions.

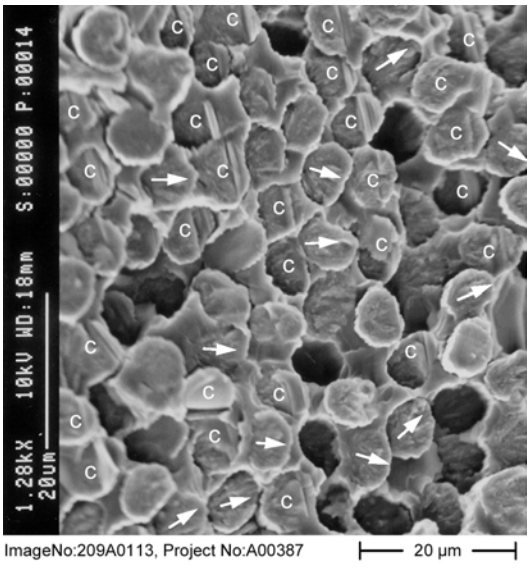

Figure 8: Fractured carbon fibers showing compression chop marks (C).

At high magnification, fiber end fractures for fibers oriented perpendicular to the fracture plane generally showed radial fracture features consistent with fracture under tensile loading. In an area near the outboard surface of the left center lug, fiber ends showed chop marks (lines across the fractured fiber ends), indicative of local compressive loading. Examples of these chop marks can be seen in Figure 8 on the fiber ends marked with a "C". The combination of tension on the inside edge and compression on the outboard surface is associated with an overall lug bending to the left. Using the radial patterns on the lug translaminar fractures, fracture propagation directions were determined to be extending from the lug holes for the right aft, right forward, and left forward lugs (all lugs that had fractures intersecting the lug hole). For the right center lug, fracture propagated from aft to forward, and for the left center and left aft lugs, fracture propagated from forward to aft.

Samples of the delamination fracture surfaces were examined in the scanning electron microscope to determine the orientation of the shear stress at the fracture and to identify the direction of crack propagation. Fracture features that were used to make these determinations included hackles (thin plates of fractured matrix material between fibers oriented perpendicular to the fiber axis, with free edges that point in a general direction opposite to the local shear applied at the fracture surface) [15, 16] and river marks (related to the initiation of matrix cracks that coalescence into larger cracks, indicating the direction of propagation) [4]. A typical view of hackles and river marks observed on one of the delaminations is shown in Figure 9. The samples also were carefully examined for indications of fatigue crack propagation, such as striations in the fiber impressions in the matrix [5, 12], matrix rollers (pieces of fractured matrix material rolled into cylindrical shapes by the relative motion of the fracture surface during cyclic loading) [5, 12], or rubbed hackle formations [5], however no evidence of fatigue was observed on any of the delamination surfaces.

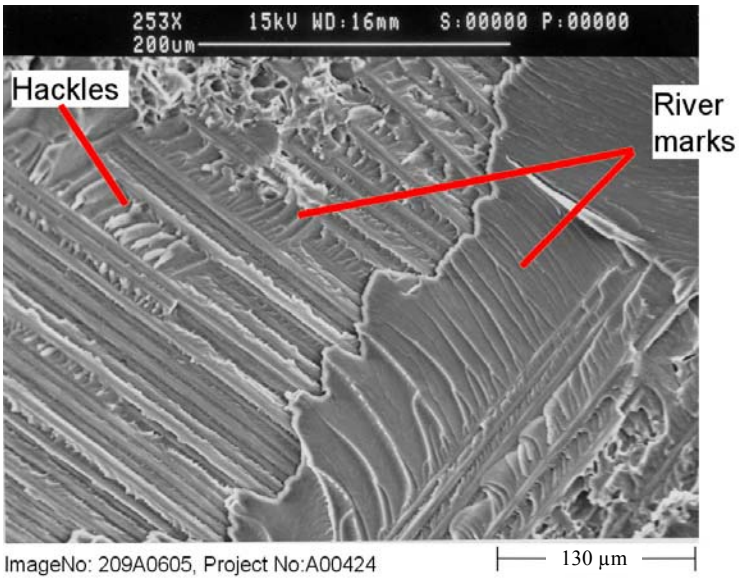

Figure 9: Delamination fracture features.

When hackles form in CFRP's, the hackles orient perpendicular to the fiber axes, so the hackles in the orthogonal bundles of the woven fabric would generally point in two orthogonal directions. In some cases, the superimposed imprints of unidirectional tape at 45° to those bundles also added hackles at a third direction. Hackles also point generally opposite the locally applied shear at the fracture surface, so the multiple orientations of hackles from the different fiber bundles bound the direction of the local shear within an angle of 90°.

River marks were observed in matrix-rich areas in the vicinity of the bundle crossings, and could be seen in the base of hackles in the transition from a bundle at one orientation to a perpendicular crossing bundle. The river marks in the matrix-rich bundle crossings were used to identify a general direction of fracture propagation upward and aftward for both of the large delaminations (at the forward left and aft left attachments). The use of the river marks at the base of the hackles to determine delamination growth direction was explored in the examination of the delaminations at the forward right lug.

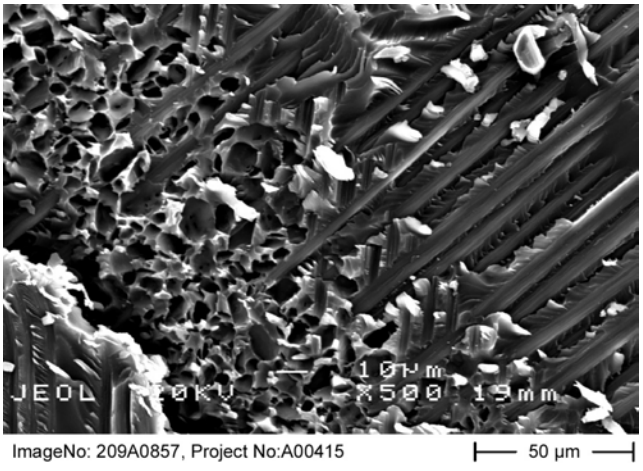

Figure 10: Porosity in matrix rich regions where bundles cross.

At the matrix-rich areas where bundles crossed, some porosity was observed having a somewhat angular appearance as shown in Figure 10. These pores were identified as arising from excess curing agent that had crystallized within the matrix. Such crystals

could have been physically removed in the fracture process or dissolved by the water from which the vertical stabilizer was recovered.

On the delamination surfaces at the left forward lug, hackles on average pointed downward and forward on the outboard side of the delamination and upward and aft on the mating side, indicating a shear direction consistent with fracture under tensile loading and/or bending to the left. River patterns coalesced upward and aft, indicating crack propagation extending upward from the lower end.

On the delamination surfaces at the left aft lug, hackles on average pointed downward and forward on the side of the delamination associated with the lug layers, and on average pointed upward and aft on the mating sides, consistent with the lug pieces moving downward relative to the remaining structure. In the portion of the delamination above the lug-to-skin transition, hackles generally pointed downward and forward on the outboard side and upward and aft on the mating side, indicating a shear direction consistent with fracture under bending to the left. River patterns generally coalesced upward and aft, indicating crack propagation extending upward from the lower end. No evidence of fatigue, such as striations in the matrix or edge rounding of the fiber ends on the translaminar fracture surfaces or matrix rollers or striations on the delamination surfaces, was observed on any of the fractures.

A summary of the observed fracture patterns is shown in Figure 11. The schematic drawing represents a horizontal cross-section of the vertical stabilizer through the main attachment lugs as viewed from above. Lug cross-sections with a light band at the center represent the lugs that failed through the bolt hole. Solid lug cross-sections represent fractures above the bolt holes. Arrows on the lug surfaces indicate the approximate direction of fracture observed on the translaminar surface. On the left center lug, the area of compression fracture features near the outboard side is indicated. The results showed that the failure pattern of fracture in tension on the right side was consistent with an overall bending of the vertical stabilizer to the left. On the left side, the failure pattern of tension and bending to the left was consistent with an overall bending of the vertical stabilizer to the left after fracture of the lugs on the right side.

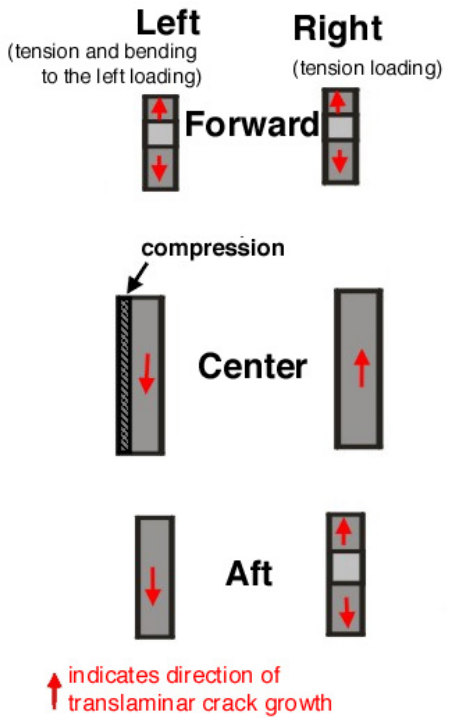

Figure 11: Main lug fracture pattern summary (viewed from above).

It was noted that the only compression translaminar failure features were present on the vertical stabilizer at the outboard side of the center aft lug. Typically, composites have less strength in compression than tension. However, the design of the vertical stabilizer was such that the magnitude of the load needed to fail a lug in tension was less than the load needed to fail the lug in compression. Furthermore after failure of the lugs on the right side, the curvature of the panel would cause tension loading in the forward and aft lug and compression in the center lug with continued bending to the left. Other unknown factors, such as changes in air loading as the vertical stabilizer deflected after the initial fractures on the right side, would further influence the failure patterns on the left side.

Subcomponent Tests

Structural analysis indicated that under accident loading conditions, fracture of the vertical stabilizer would have initiated at the right aft lug. Three aft lugs were obtained for mechanical testing under

applied loads that were derived from recorded flight data from the accident. The lug for the first test was obtained from a production left skin panel that had sections cut from it for destructive testing, but the aft lug had been left undisturbed. The lugs for the second and third tests were obtained from a vertical stabilizer that had been removed from service after experiencing loads exceeding design limit loads. The three vertical stabilizer aft lug specimens were tested at Airbus Industrie under National Transportation Safety Board supervision in a loading fixture that applied prescribed forces and moments to the lugs. Testing of each lug continued until a load change associated with a translaminar fracture or crack was observed. The fracture loads for these three tests were consistent with calculated accident loads and with earlier tests completed by Airbus Industrie during certification. Details of the test procedures and results are documented in references 17-21. A fractographic examination of each of the lugs was conducted after completing the tests as documented in reference 22.

Before testing, each lug was examined for non-visible defects or damage using ultrasonic inspection. Results of these inspections are documented in reference 22. No defects were observed in the first test lug. Some damage was detected in the second and third test lugs near the lug attachment hole and in some areas in the lug fitting assembly transition area above the lowermost rib, however these lugs had experienced in-service loads exceeding design limit loads. Following the tests, the lugs were examined again using ultrasonic inspection. The post-testing ultrasonic inspection showed that the preexisting damage in these lugs grew in size during the testing.

Overall views of the lugs from each test are shown in Figure 12 (outboard surface view). A similar view of the accident right aft lug also is shown in Figure 12. Unlabeled red arrows indicate where translaminar cracks or fractures intersected the outboard surfaces of the lugs, and an unlabeled large green arrow indicates loading direction (the force vector for the horizontal and vertical loading components for each lug). The lugs from the first and second tests were left aft lugs, and as such, the orientations are mirror images of the accident right aft lug and the third test lug.

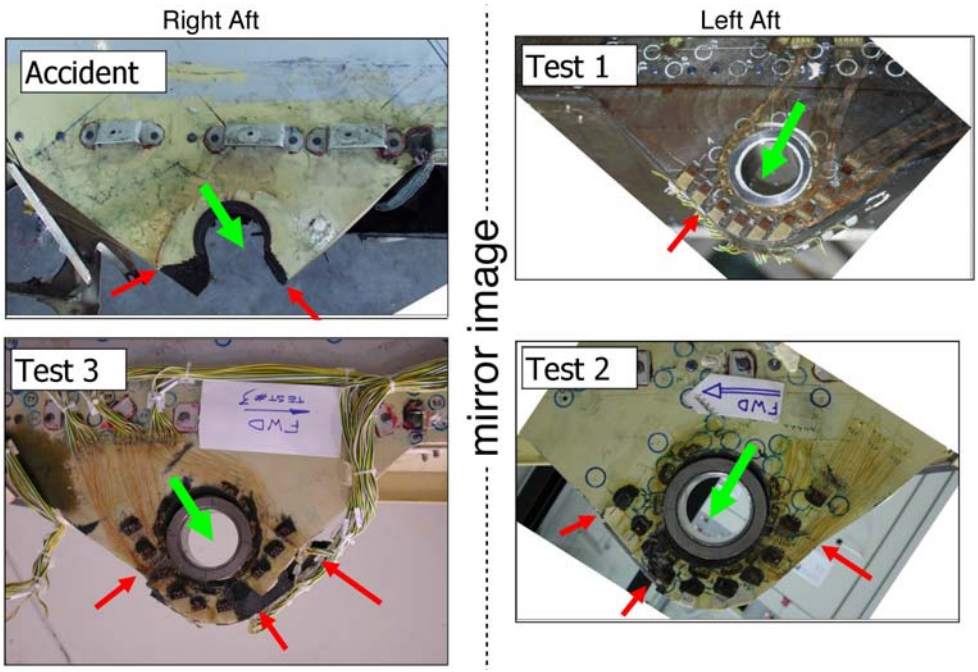

Figure 12: Aft lugs from accident and subsequent subcomponent tests.

Results from the fractographic examination showed that fractures in the test lugs occurred at locations similar to those on the accident right aft lug. In the first test, loading was interrupted after a translaminar crack occurred at the location indicated by the red arrow in the upper right photo in Figure 12. The translaminar fracture was located at a position on the forward part of the lug in a plane nearly parallel to the resultant force direction, similar to one of the translaminar fractures in the accident right aft lug. Fracture features for the lugs from tests 2 and 3 were similar to each other. The outboard side of each of these lugs had a translaminar fracture on the forward sides of the holes in a plane nearly

parallel to the loading direction and another translaminar fracture at the aft side of the hole in a plane approximately perpendicular to the loading direction, fractures similar to that of the accident lug. In addition on the outboard sides, a compression buckling fracture was observed on the forward sides of each lug above the fracture parallel to the loading direction, which is different from features on the accident lug but was attributed to constraints of the loading fixture. On the inboard sides of lugs 2 and 3, fracture locations were on translaminar planes different from that of the outboard side of the lug. This change in fracture planes was similar to that of the accident right aft lug.

A delamination was present within the first test lug having an extent similar to that of the accident right aft lug and in a location through the thickness slightly outboard of that of the accident right aft lug. Delaminations also were detected above the translaminar fractures in lugs 2 and 3. In lugs from tests 2 and 3, the locations of the delaminations through the thickness were similar to that of the accident right aft lug, but the extents of the delaminations in the test lugs were slightly less.

Each subcomponent test lug had translaminar fractures that intersected the lug hole and had delaminations that were located within the lug, features similar to the accident right aft lug. Each lug had a translaminar fracture at the forward lower side of the hole on the outboard side of the lug, including the first test, which was interrupted and had no other translaminar fractures. The fracture at the forward lower side of the hole corresponds to one of the translaminar fracture locations on the accident lug. The second test lug showed changes in translaminar fracture planes that were qualitatively similar to that of the accident right aft lug. These results indicated that the accident right aft lug had fracture features consistent with being the first lug fracture from a substantially intact vertical stabilizer and rudder under accident load conditions.

Concluding Remarks

The materials testing and microstructural examination of the vertical stabilizer indicated the vertical stabilizer's composite material had sufficient cure, desired fiber volume fraction, and acceptable void content with no evidence of microcracking in the areas examined. Discrepancies representing a small fraction of the total number of layers were observed in the layup of one of the samples. However, throughout the testing and examination, no deviations from the original design and materials specifications were found that would have contributed to the vertical stabilizer separation.

The fractographic examination revealed no evidence of pre-existing damage or fatigue cracking in the vertical stabilizer, supporting the conclusion that the separation of the vertical stabilizer was a result of high aerodynamic loads. The fractographic results of examination of the main attachment lugs for the vertical stabilizer showed that failures on the right side of the vertical stabilizer were overstress failures under tension loading, consistent with an overall bending of the vertical stabilizer to the left. Fractographic results for the main lugs on the left side of the vertical stabilizer showed overstress failure in tension and bending to the left, consistent with bending of the vertical stabilizer to the left after failure of the main lugs on the right side. The structural analysis of the vertical stabilizer also conducted as part of the overall investigation indicated that under accident loads, fracture of the vertical stabilizer would initiate at the right aft main lug, which was consistent with the fractographic analysis.

The failure mode in the accident was further confirmed by a series of three aft lug subcomponent tests. The failure loads for these three tests were consistent with predicted failure loads and with earlier tests completed by Airbus Industrie during certification. Fracture patterns for the three test specimens were compared to the corresponding structure on the accident airplane, and good correlation was observed.

The analysis of the fractographic evidence was incorporated into the overall analysis of the accident. As one of the findings of the Safety Board's report stated, "Flight 587's vertical stabilizer performed in

a manner that was consistent with its design and certification. The vertical stabilizer fractured from the fuselage in overstress, starting with the right rear lug while the vertical stabilizer was exposed to aerodynamic loads that were about twice the certified limit load design envelope and were more than the certified ultimate load design envelope [1]."

References

1. NTSB, *Aircraft Accident Report, In-Flight Separation of Vertical Stabilizer*, NTSB/AAR-04/04, NTSB Public Docket, 2004.

2. NTSB, *Materials Laboratory Factual Report 02-082*, NTSB Public Docket, 2002.

3. Mills, K., et.al., ed. *Fractography, ASM Handbook Vol. 12*. 1987, ASM International: Metals Park, Ohio.

4. Kar, R.J., *Atlas of Fractographs*, in *Composite Failure Analysis Handbook Volume 2: Technical Handbook*. 1992, Northrop Corp, Aircraft Div.

5. Sjögren, A., L.E. Asp, and E.S. Greenhalgh, *Interlaminar Crack Propagation in CFRP: Effects of Temperature and Loading Conditions on Fracture Morphology and Toughness*, in *Composite Materials: Testing and Design, and Acceptance Criteria, ASTM STP 1416*, Nettles and Zureick, Editors. 2002.

6. NTSB, *Materials Laboratory Factual Report 02-077*, NTSB Public Docket, 2002.

7. NTSB, *Materials Laboratory Factual Report 02-083*, NTSB Public Docket, 2002.

8. NTSB, *Materials Laboratory Factual Report 03-018*, NTSB Public Docket, 2003.

9. NTSB, *Materials Laboratory Factual Report 02-078*, NTSB Public Docket, 2002.

10. NTSB, *Materials Laboratory Factual Report 03-033*, NTSB Public Docket, 2003.

11. Purslow, D., *Matrix Fractography Of Fibre-Reinforced Thermoplastics, Part 2. Shear Failures.* Composites Vol. 19, 1988.

12. Stumpff, P.L., *Fractography*, in *ASM Handbook, Vol. 21: Composites*. 2001. p. 977-987.

13. Stumpff, P.L., *personal communication*. 2002.

14. Mandell, J.F., *Fatigue Behavior of Short Fiber Composite Materials*, in *Fatigue and Fracture of Composite Materials*, K.L. Reifsnider, Editor. 1990, Elsevier. p. 231-337.

15. Singh, S. and E. Greenhalgh. *Micromechanisms of Interlaminar Fracture in Carbon-Epoxy Composites at Multidirectional Ply Interfaces.* in *4th International Conference on Deformation & Fracture of Composites*. 1998. Manchester, UK: UMIST.

16. Hibbs, M.F. and W.L. Bradley, *Correlations Between Micromechanical Failure Processes and the Delamination Toughness of Graphite/Epoxy Systems*, in *Fractography of Modern Engineering*

Materials: Composites and Metals, ASTM STP 948, J.E. Masters and J.J. Au, Editors. 1987, American Society for Testing and Materials: Philadelphia. p. 68-97.

17. NTSB, *Structures Group Factual Report Addendum 17*, NTSB Public Docket, 2004.

18. NTSB, *Structures Group Factual Report Addendum 16*, NTSB Public Docket, 2004.

19. NTSB, *Structures Group Factual Report Addendum 15*, NTSB Public Docket, 2004.

20. NTSB, *Structures Group Factual Report Addendum 8C*, NTSB Public Docket, 2004.

21. NTSB, *Structures Group Factual Report Addendum 6 (Rev A)*, NTSB Public Docket, 2004.

22. NTSB, *Materials Laboratory Factual Report 04-065*, NTSB Public Docket, 2004.